Chem Soc Rev

The electronic structure calculations of two-dimensional transitionmetal dichalcogenides in the presence of external electric and magnetic fields

Journal:	*Chemical Society Reviews*
Manuscript ID:	CS-REV-08-2014-000276.R1
Article Type:	Tutorial Review
Date Submitted by the Author:	17-Aug-2014
Complete List of Authors:	Kuc, Agnieszka; Jacobs University Bremen, SES Heine, Thomas; Jacobs University Bremen, School of Engineering and Science

The electronic structure calculations of two-dimensional transition-metal dichalcogenides in the presence of external electric and magnetic fields

Agnieszka Kuc[*a] **and Thomas Heine**[*a]

Received Xth XXXXXXXXXX 20XX, Accepted Xth XXXXXXXXX 20XX
First published on the web Xth XXXXXXXXXX 200X
DOI: 10.1039/b000000x

Transition-metal dichalcogenides TX_2 (T = W, Mo, X = S, Se, Te) are layered materials that are available in ultrathin forms such as mono-, bi- and multilayers, which are commonly known as two-dimensional materials. They have an intrinsic band gap in the range of some 500 meV to 2 eV, depending on composition and number of layers, giant intrinsic spin-orbit splittings for odd layer numbers, and, in conjunction with their high chemical and mechanical stability, they qualify as candidate materials of two-dimensional flexible electronics and spintronics. The electronic structure of each TX_2 material is very sensitive to external factors, in particular towards electric and magnetic fields. A perpendicular electric field reduces the band gap, and for some structures semiconductor-metal transitions could be possible. Moreover, the electric field triggers the spin-orbit splitting for bilayers. A magnetic field applied normal to the layers causes the Hall effect, which in some cases may result in a quantum (spin) Hall effect and thus in magnetic switches. Finally, we discuss how valleytronics is possible in these materials by selective interaction of electrons in the different valleys using polarized light.

1 Introduction

The raise of graphene as prototype two-dimensional (2D) material[1] has triggered enormous research efforts in order to develop truly 2D applications, in particular in flexible electronics. Graphene has attracted worldwide interest because of its high electron mobility, exceptional electronic and mechanical properties, long-distance spin-transport and massless Dirac fermions. It has, therefore, great potential as a spin-conserving system in spintronic devices. Pristine graphene is a zero band-gap semiconductor and its intrinsic inversion symmetry strongly suppresses the spin-orbit coupling (SOC). Thus, graphene cannot be used as a switching material in spin- or charge-based transistors. Ultrathin transition-metal chalcogenides (TMCs) include semiconductors with giant spin-orbit coupling and are therefore complementary to graphene and to the 2D prototype insulator, hexagonal boron nitride *h*-BN.

Due to the recent development of advanced exfoliation techniques many layered materials can be prepared as monolayers (MLs), and their large variety in terms of structure and composition offers a wide range of intrinsic electronic properties.[2–6] It is of particular interest that some TMCs offer special electronic properties only as MLs that are distinct from their bulk or multilayer forms, for example TMCs of the TX_2 type (T = Mo, W; X = S, Se, Te).[7–9] For MoS_2, a series of 2D electronic devices has been manufactured in the laboratory, among them transisitors, optical sensors, logical switches etc.[2,10]

Layered TX_2 TMCs in bulk form have been extensively studied on experimental and theoretical bases for the last 50 years. A TX_2 ML contains three atomic layers, X-T-X, with the transition metal atom covalently bonded to six chalcogen atoms, forming a sandwiched material (Figure 1). In the bulk, the MLs are stitched together by weak interlayer interactions, allowing easy exfoliation. TMCs exist predominantly in three polymorphs (see Figure 1 a),[4] i.e. 1*T*, 2*H* and 3*R*. Here, the letters label trigonal, hexagonal and rhombohedral, respectively, and the numbers indicate the number of layers in the unit cell. Molybdenum disulfide (MoS_2) is a natural mineral, predominantly available in 2*H* form with trigonal prismatic coordination of the metal atoms. Synthetic MoS_2 may contain also the 3*R* phase, while Li intercalation may lead to the metallic 1*T* form.[11] The 1*T* polymorph is, however, typically observed for group 4 TMCs, e.g. TiS_2, with octahedral metal atom coordination. In the following, we will restrict our review to the MLs and bilayers (BLs) of semiconducting TMCs in the 2*H* form, unless otherwise stated. For more details on all three polymorphs, the reader is refereed to the recent reviews.[3–5]

2*H* TMCs belong to the space group $P6_3/mmc$ D^4_{6h} (no. 194). Two equivalent transition-metal atoms are placed at the 2*c* sites (±1/3, ±2/3, ±1/4), while four equivalent chalcogen

[a] *School of Engineering and Science, Jacobs University Bremen, Campus Ring 1, 28779 Bremen, Germany. Fax: +49 421 200 49 3223; Tel: +49 421 200 3223; E-mail: a.kuc@jacobs-university.de; t.heine@jacobs-university.de*

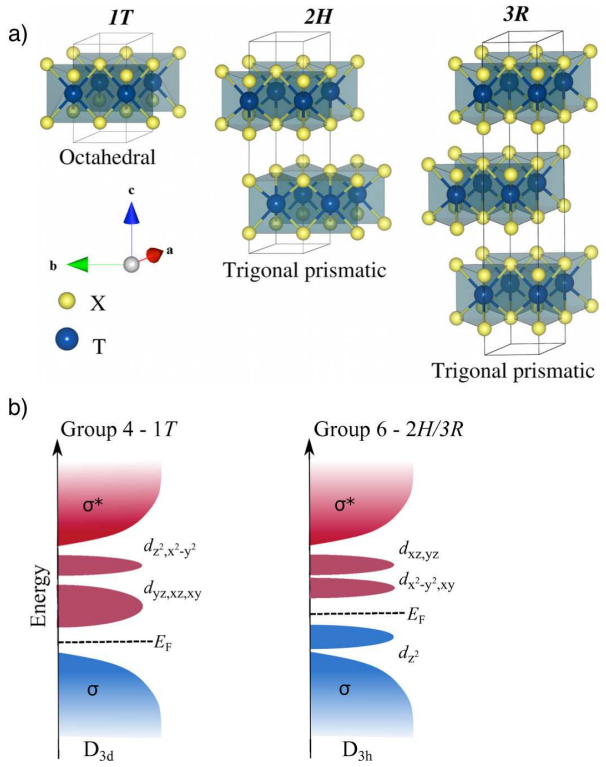

Fig. 1 (a) Structural representation of 1*T*, 2*H* and 3*R* TMC polytypes together with their metal atom coordination. The numbers indicate the number of layers in the unit cell and the letters stand for trigonal, hexagonal and rhombohedral, respectively. (b) Schematic representation of the density of states of selected transition-metal groups. The corresponding *d*-orbital splitting due to the symmetry is indicated.

atoms are at the 4*f* sites (±1/3, ±2/3, ±*u*) and (±1/3, ±2/3, ±(*u*+1/2), with $u = 0.63$).[12] When the 3D TMC bulk is reduced to the MLs, the trigonal prismatic coordination is still maintained, but the symmetry is reduced to $P\bar{6}m2$ D^1_{3h} (no. 187).

Depending on the number of *d*-electrons of the transition metal atom, the TX_2 systems can be metallic, semiconducting or insulating, with a wide range of magnetic properties. Octahedral coordination (D_{3d}) results in two sets of degenerate *d*-orbitals, d_{z^2,x^2-y^2} and $d_{xy,xz,yz}$, while in the trigonal prismatic configuration (D_{3h}) the *d*-orbitals split into three groups: d_{z^2}, $d_{x^2-y^2,xy}$ and $d_{xz,yz}$ (see Figure 1 b).

TMCs in 2D form have become important only very recently, when Nicolosi and co-workers have shown that large area TMC MLs can be easily produced via liquid exfoliation.[13] Quantum confinement of bulk TMCs to 2D MLs and BLs causes significant changes in the structural, electronic and optical properties.[7–9,14] First of all, TMC MLs, similar to graphene, are not expected to be completely flat. This has been shown on the experimental and theoretical basis for the free-standing MoS_2 ML,[15,16] however, it should also hold for the other TMCs. Brivio et al.[15] reported intrinsic ripples in the microscopic structure of MoS_2 MLs of height in the range of 6-10 Å for the lateral length of flakes 6-10 nm. This observation was supported by Born-Oppenheimer molecular dynamics simulations by Miró et al.,[16] who showed that the inherent dynamics of MoS_2 MLs leads to the spontaneous formation of ripples already at low temperatures. The theoretically obtained ripples converged to the heights observed experimentally for supercells with the lateral lengths of about 9 nm.

Ever since the successful production of MLs, several interesting and intriguing properties of TMCs have been discovered and discussed in the literature,[7,8,17–26] including the size-dependent band gaps and Raman peak shifts, tensile strain induced semiconductor-metal transition, band gap closure of BLs in an external electric field, giant spin-orbit splitting, spin-valley coupling, Rashba and out-of-plane Zeeman effects, and many others. Some of the mentioned phenomena have been first predicted from quantum mechanical simulations and subsequently supported by experiments.

In this tutorial review, we discuss the electronic structure changes of 2D semiconducting TMC materials in the presence of external fields, starting with the theoretical background, such as Rashba, Stark or Zeeman effects in 2D materials. We will show the importance of carefully choosing the quantum methods and structural models to correctly simulate and describe these phenomena. This review is organized as follows: in Section 2 we will discuss the intrinsic electronic properties of TMC MLs and BLs; in Section 3 we will show the influence of an electric field applied normal to the layer on these properties and the resulting Stark effect; Section 4 will focus on the simulations of heterostructures and the Rashba effect that arises from the perpendicular potential gradient; in Section 5, we will introduce the electronic structure influenced by an external magnetic field and the magnetoelectric effects; and finally in Section 6, we will discuss the spin and valley Hall effects. We will avoid the discussion of finite systems such as flakes and nanoribbons, as their electronic properties are governed by the edges and difficult to control in experiment.

2 Intrinsic Electronic Properties

When semiconducting 2*H* TMCs are confined from the bulk to the MLs, their crystal symmetry lowers and consequently their electronic structure changes significantly. TMC films with even number of layers (including bulk and BLs) exhibit inversion symmetry with the inversion centre between the layers, which is explicitly broken in systems with odd number of layers (including MLs), as shown in Figure 2. Therefore, TMC MLs exhibit a couple of important phenomena that are required for applications in modern nanoelectronics: Firstly,

hexagonal symmetry imposes the existence of inequivalent valleys with the same energy, but different momentum (K and K'); secondly, due to lack of inversion symmetry, SOC causes valence band splittings [17,27] for which the spin projections are defined as spin up and spin down. The valley degree of freedom in MLs for low-energy carriers is robust against low-energy phonons because of the large separation of K and K' in momentum space. The energy valleys are subject to the optical selection rule, [19–22] which states that the left (right)-handed circularly polarized light σ- (σ+) couples to the band-edge transitions at K (K') due to angular momentum conservation and time-reversal symmetry. The broken spin degeneracy and time-reversal symmetry imply inherent spin-valley coupling (SVC) in the MLs. The SVC forbids independent spin or valley flipping, anticipating long valley-spin lifetimes for holes, [19] a feature utilized in spin- and valleytronic applications. In the centro-symmetric TMC BLs, the spin degeneracy of the valence bands is restored by spatial inversion and time-reversal symmetries, and SOC is strongly suppressed. This leads to decoupling between valley and spin degrees of freedom, which means that under circularly polarized light, both valleys are equally populated and only a net spin is produced. The absence of valley-specific excitations arises from the BL symmetry and results in a weak photoluminescence helicity. [22] Furthermore, due to the mirror symmetry in TMC layers, the sum of potential gradients normal to the planes is zero, thus forbidding the occurrence of the Rashba effect.

In the following, we will discuss the intrinsic electronic properties of TMC materials on the basis of computational results in more detail: For all TMCs of the form TX_2 (T = Mo, W, X = S, Se), decreasing the number of layers results in the transition from being an indirect band gap (bulk to BL) to a direct band gap semiconductor in the ML (see Figure 3). [7–9] In the MoS_2 example, the indirect band gap is in the near-infrared frequency range (Δ = 1.3 eV), while the direct band gap shifts to the range of the visible light (Δ = 1.9 eV). [9] Increasing the size of the chalcogen atom decreases Δ to about 1.0 eV for the $MoTe_2$ bulk [28] or to 1.4 eV for the $MoTe_2$ ML. [29] The indirect-to-direct band gap transition is manifested in the enhanced photoluminescence of MLs compared with a very weak emission in multilayered systems. [7,8] Such layer-dependent electronic properties have recently attracted a great attention for possible applications in nano- and optoelectronics. [2]

The calculation of structural and electronic properties of TMCs is somewhat intriguing, it requires some attention to chose the appropriate quantum method to describe the envisaged phenomena. Density-functional theory (DFT) has been widely used for electronic structure calculations in the fields of materials science, chemistry and physics. The choice of exchange-correlation functional and orbital basis is crucial to obtain correct description of the crystal structure and electronic structure. While the covalent intralayer bonding of TMCs is well reproduced with nearly any density functional (e.g. PBE), the interactions between the layers should be treated with a suitable model to correct for the missing weak London dispersion forces. Typically, these weak interlayer forces are accounted for by a force-field like correction. Although the weak dispersion interactions are not directly reflected in the electronic structure, they strongly affect the crystal structure, which in turn may completely change the information about Δ, namely too large (too short) interlayer distance result in overestimated (underestimated) energy band gaps. [30]

In general, DFT calculations give very good band structures and effective masses of electrons and holes, however, the band gaps might not be well reproduced as compared with the experimental data or higher-level methods. The most common issue is the underestimation of band gaps, what can be corrected, e.g. by model exchange correlation potentials, such as the Tran-Blaha modified Becke-Johnson (TB-mBJ) potential, or by more accurate methods, like e.g. the GW approximation. It should be taken into account, however, that for semiconducting TMCs, we have obtained band gaps in a good agreement with experiment using the PBE functional and Gaussian-type basis functions. [9] This is because of an error cancellation: due to quenched Coulomb screening that has been explored in detail for graphene, [31] 2D materials have large exciton binding energies that roughly compensate the band gap underestimation at the DFT/PBE level.

Using a plane wave approach and the PBE functional, Wei et al. [32] obtained a somewhat smaller Δ of 0.79 eV for bulk MoS_2. For the same system, Matte et al. [33] reported 1.10 eV, using the PBE functional with a DZP basis set. Using the Perdew-Wang exchange-correlation functional (PW91) and a self-consistent pseudopotential, Arora et al. [34] reported an indirect band gap of 1.32 eV for 2H WS_2, in very close agreement with our PBE results. [9] In the cases of MoS_2 (WS_2) MLs, Johari et al. [29] reported 1.68 (1.81) eV at the PBE/PAW level, and Ataca et al. [35] obtained 1.87 and 2.57 eV (1.98 and 2.84 eV) from the LDA/PAW and GW_0 calculations, respectively. The experimental bulk and ML band gaps reported for MoS_2 (WS_2) by Kam et al. [36] are 1.23 and 1.69 eV (1.35 and 1.74 eV), respectively.

TMC materials consist of heavy elements and the relativistic treatment of the core electrons is of great importance. Moreover, the spin-orbit (SO) interactions can significantly alter the electronic structure (see Figure 4). All TMC MLs of the form TX_2 (T=Mo, W, X=S, Se) are direct band gap semiconductors. The valence band maximum (VBM) and the conduction band minimum (CBM) are predicted to be at the high-symmetry K point, irrespective whether or not the relativistic effects were taken into account. [37] However, within the non relativistic (NR) calculations of the MoS_2 ML, we have obtained the VBM at the Γ point. Here, the K point is situated

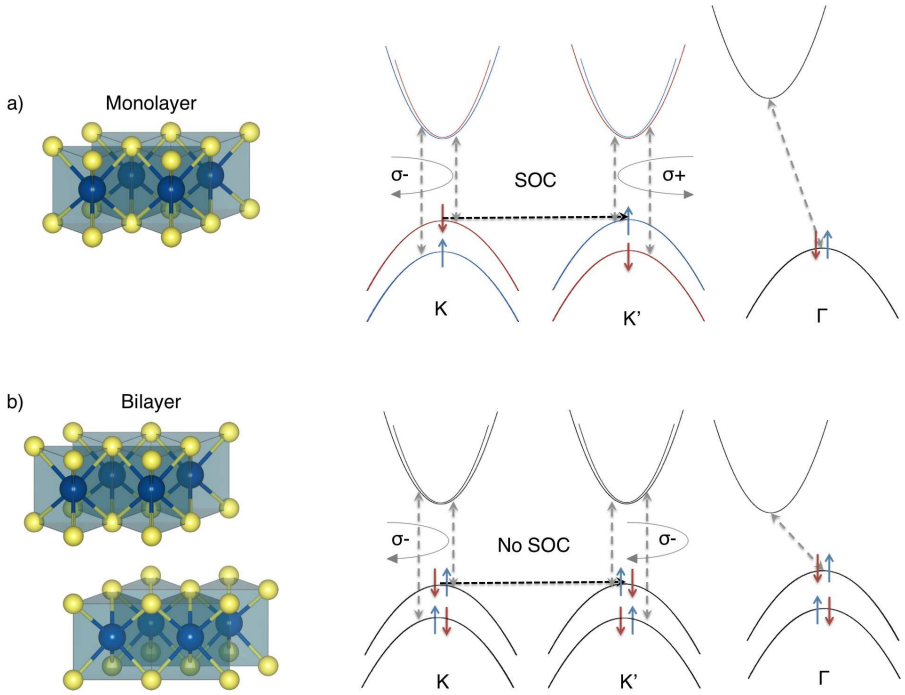

Fig. 2 Schematic representation of a 2*H* TMC monolayer (ML; a) and bilayer (BL; b) together with the valence band maximum (VBM) and conduction band minimum (CBM). (a) The spatial inversion symmetry is broken in TMC MLs. The spin degeneracy at the VBM is lifted by the spin-orbit coupling (SOC). The valley and spin degrees of freedom are coupled. Valley-dependent optical selection rule: left (right)-handed circularly polarized light σ- (σ+) couples to the band-edge transitions at K (K') due to angular momentum conservation and time-reversal symmetry. (b) The spin degeneracy is restored by spatial and time-reversal symmetries. No spin-valley coupling is present. Under circularly polarized light both valleys are equally populated. Note, in BLs there are twice as many bands as in MLs in the electronic structure. BLs are indirect and MLs are direct band gap (Δ) semiconductors. Blue and red bands are spin-polarized.

42 meV lower in energy than the Γ point.

Scalar relativistic (SR) calculations, within the zero order relativistic approximation (ZORA), overestimate Δ comparing with the SR+SO (scalar relativistic with spin-orbit interactions) results by 60-280 meV depending on the TMC composition. This difference is larger for heavier chalcogen and transition-metal atoms.

Quantum calculations on TMC MLs reveal SO splittings (Δ_{SO}) of several hundred meV in the VBM. Larger Δ_{SO} values, as expected, are obtained for TMCs with heavier elements, going from about 150 meV to nearly 500 meV for MoS_2 and WTe_2, respectively (see Table 1).[17,26,37] These numbers change only slightly between simulations with the TB-mBJ potential and PBE functional. Our results from Table 1 are in a very reasonable agreement with other *ab initio* calculations. From the full-potential linearized augmented-plane-wave approach at the PBE level, Zhu et al.[17] obtained the maximal spin-splitting in the VBM at the K point of 148, 183, 426, and 456 meV for MoS_2 , $MoSe_2$, WS_2, and WSe_2 MLs, respectively. Using plane-waves approach and the PBE functional, Kośmider et al.[38,39] have obtained 147 and 435 meV splitting in MoS_2 and WS_2, respectively.

The SO splitting in the CBM is much weaker than that in the VBM and its values may be strongly affected by the exchange-correlation functional used in the simulations. Our calculations show that for the MoS_2 ML, Δ_{SO}^{CBM} of 26 meV versus 12 meV was obtained from the TB-mBJ and PBE, respectively. Using the PBE and the more modern HSE functional, Kośmider et al.[38,39] have obtained 3 and 21 meV, respectively, for MoS_2. From plane-wave calculations, Cheng et al.[26] have obtained 3, 20, 34, 29, 34, and 51 meV for the MoS_2, $MoSe_2$, $MoTe_2$, WS_2, WSe_2, and WTe_2, respectively. Nearly the same results were reported by Kormányos et al.[40] However, for a better description methods beyond ground-state DFT are required.

TMC materials have very interesting electronic structures which depend strongly on the number of TMC layers in the system. The electronic structure can be strongly affected by external stimuli, such as in-plane tensile strain,[14] electric or magnetic fields perpendicular to the basal planes. The latter will be discussed in the next sections.

Table 1 Calculated energy band gaps (Δ), spin-orbit splitting (Δ_{SO}) of the valence band maximum (VBM) and the conduction band minimum (CBM) at the *K* point of TMC MLs. Note: data using SO calculations, Ref. 37 - numerical and Slater-type basis functions, Ref. 26 - plane-wave approach.

System	TB-mBJ[37]			PBE[37]			PBE[26]		
	Δ (eV)	Δ_{SO}^{VBM} (meV)	Δ_{SO}^{CBM} (meV)	Δ (eV)	Δ_{SO}^{VBM} (meV)	Δ_{SO}^{CBM} (meV)	Δ (eV)	Δ_{SO}^{VBM} (meV)	Δ_{SO}^{CBM} (meV)
MoS_2	1.62	147	26	1.61	147	12	1.65	150	3
$MoSe_2$	1.40	176	34	1.39	180	29	1.38	188	20
$MoTe_2$	0.97	190	46	0.94	209	46	1.00	219	34
WS_2	1.74	395	17	1.59	419	10	1.68	431	29
WSe_2	1.43	428	3	1.23	449	24	1.32	473	34
WTe_2	0.86	480	4	0.77	476	26	0.85	493	51

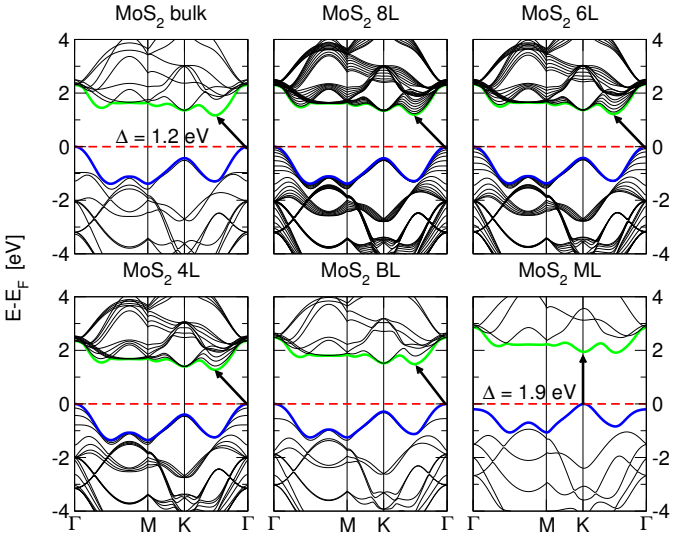

Fig. 3 Band structures of MoS_2 going from bulk to monolayer (ML). Number of layers is indicated for each structure. Calculations at the DFT/PBE level without relativistic effects. The horizontal dashed lines indicate the Fermi level. The arrows indicate the fundamental band gap. The top of valence band (blue) and bottom of conduction band (green) are indicated. Results taken from Ref. 9. Indirect-direct band gap transition is encountered when going from BL to ML structure. A similar phenomenon is observed for other semiconducting TMCs.

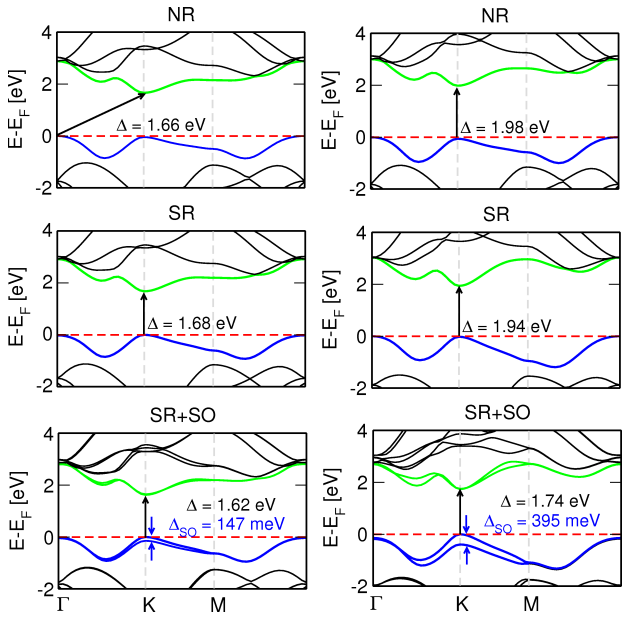

Fig. 4 Band structures of Mo_2 (left) and WS_2 (right) monolayers calculated at the DFT/TB-mBJ level. Fundamental band gaps (Δ) and spin-orbit splittings (Δ_{SO}) are given. NR-non relativistic, SR - scalar relativistic, SR+SO - scalar relativistic with spin-orbit interactions. Results taken from Ref. 37

3 The Influence of an External Electric Field on the Electronic Structure of 2D TMC

Wu et al.[41] suggested that the inversion symmetry in TMC BLs can be broken by an external electric field, which leads to a potential gradient between individual layers, and allows the control over valley polarization. This effect should be even more pronounced for TMCs with stronger SO splittings.[6] In an electronic device, an electric field is conveniently introduced to a 2D system by a gate voltage, and strong fields can be achieved using ionic-liquid gating. This is particularly useful in 2D materials as the field is oriented perpendicularly to the planes. In a recent example, Yuan et al.[24] have shown that the out-of-plane Zeeman-type spin polarization in WSe_2

BL-based transistor can be induced using an ionic-liquid-gate voltage.

Spin-orbit coupling is a relativistic effect that originates from the coupling between spin ($\boldsymbol{s}$) and momentum ($\boldsymbol{p}$) of particles in an external electric field ($\boldsymbol{E}$). The SOC Hamiltonian can be written as:

$$\hat{H}_{SO} = -\mu_B \boldsymbol{s} \cdot \left[\frac{\boldsymbol{p} \times \boldsymbol{E}}{2m^* c^2} \right] \quad (1)$$

where $\boldsymbol{s}$, μ_B, m^* and c are spin Pauli matrices ($\boldsymbol{s}_{x,y,z}$), Bohr magneton, carrier effective masses and speed of light, respectively. The effective magnetic field is defined as:

$$\boldsymbol{B}_{eff} = \frac{\boldsymbol{p} \times \boldsymbol{E}}{2m^* c^2}. \quad (2)$$

Its strength, and thus the resulting spin-polarization, depend on $\boldsymbol{p}$ and $\boldsymbol{E}$, and their relative directions.[42,43] This general definition can now be adapted to the special case of 2D TMC layered materials with, as in the case of our focus materials, D_{3h} symmetry. Following the minimal band model of Xiao et al.,[19] the SOC Hamiltonian can be written for MLs:

$$\hat{H}_{SO} = \boldsymbol{a}\, t \cdot (\tau k_x \sigma_x + k_y \sigma_y) + \frac{\Delta}{2}\sigma_z - \lambda\, \tau \frac{\sigma_z - 1}{2} \boldsymbol{s}_z \quad (3)$$

where $\boldsymbol{a}$ is the lattice constant, t is the effective hopping integral, $\tau = \pm 1$ is the valley index, (k_x, k_y) is the relative wave vector between the K and K' points in the Brillouin zone, and $\sigma_{x,y,z}$ are the Pauli matrices. Taking into account the C_{3h} symmetry, at the band edges the two basis functions can be written as:

$$|A\rangle = |d_{z^2}\rangle \text{ and } |B\rangle = \frac{1}{\sqrt{2}} \left(|d_{x^2-y^2}\rangle \right) + i\tau\, |d_{xy}\rangle. \quad (4)$$

Here, Δ is the band gap, 2λ is the spin splitting at the VBM, and $\boldsymbol{s}_z$ is the spin Pauli matrix, which is a good quantum number, because the spin-up and spin-down components are decoupled. Thus, the spin splitting is a general consequence of broken inversion symmetry, as time-reversal symmetry requires that the splitting has opposite sign at K and K' valleys. Using similar considerations one can derive the respective equations for BLs,[23] where the basis functions will be defined for upper and lower layer, and the interlayer hopping is included in the Hamiltonian. The Pauli matrix can be regarded as the layer pseudospin (layer electrical polarization). Depending on the direction of the effective magnetic field that arises from the external electric field, the resulting electronic structure may exhibit Rashba or out-of-plane Zeeman effects.[24]

Recently, it has been shown that the response of the electronic structure of 2D TMC materials towards an external perpendicular electric field ($\boldsymbol{E}_\perp$) is strongly system-dependent, in particular it crucially depends on the number of layers.[18,44–46] An electric field applied to a system shifts the chemical potential, allowing electrons to delocalize corresponding to the charge polarity of the gate electrodes. Consequently, $\boldsymbol{E}_\perp$ polarizes the material in such a way that dipole moments are induced perpendicular to the plane. The schematic representation of the band structure under $\boldsymbol{E}_\perp$ is shown in Figure 5 for ML and BL TMCs. The electronic structure of TMC MLs are not affected by $\boldsymbol{E}_\perp$ within field strength that are common in electronic devices. In fact, all quantities that define the electronic properties of the TMC MLs, such as Δ, effective masses of electrons and holes, or Δ_{SO}, are extremely stable in the field.

On the other hand, $\boldsymbol{E}_\perp$ changes significantly the electronic structure of BLs, namely, it polarizes the electron density and introduces an anisotropy into the system. This anisotropy also breaks the inversion symmetry, which creates SO splitting in the valence and conduction bands, due to the so-called Stark effect (cf. Figure 5 b).[47] Our calculations show that the Δ_{SO} induced in BLs reaches values that are close to those observed for corresponding TMC MLs (see Figure 6 and Table 1).[46]

Moreover, the band gap of BLs reduces nearly linearly with the applied $\boldsymbol{E}_\perp$, undergoing the semiconductor-metal transition for field strengths of about 1.2 V Å^{-1}. It is easier to modify the electronic structure of WX_2 BLs, as even weaker fields are required. For the same field strengths, Δ of TMC MLs stays unchanged and the transition to metallic character occurs only for fields as strong as 4 V Å^{-1} (6 V Å^{-1}) for selenides (sulphides). At the same time, both MLs and BLs become indirect band gap semiconductors already for relatively weak fields. This is due to the Stark effect, which causes the bands to split and shift in energy under the electric field.

In the literature, however, the calculated band gap closure in TMC BLs is reported in controversy: Ramasubramaniam and co-workers[18] have investigated the effect of $\boldsymbol{E}_\perp$ applied to various TX_2 BLs. Their first principles based plane wave calculations with spin-orbit interactions indicate that the band gap decreases linearly with $\boldsymbol{E}_\perp$, resulting in the band gap closure in the range of relatively small electric field of only 200-300 mV Å^{-1}. On the other hand, Liu et al.[44] have reinvestigated the electric field influence on the electronic structure of a MoS_2 BL, but considering different stacking configurations of molybdenum and sulphur atoms in the 2D layers, concluding that the $\boldsymbol{E}_\perp$ strength, at which the band gap closes, is significantly higher, in the range of 1.0 and 1.5 V Å^{-1}. The strongly underestimated values of Ramasubramaniam et al.[18] were probably caused by applying inappropriate constrains to the symmetry of the BLs. However, Liu et al.[44] have not accounted for the spin-orbit interactions. Nevertheless, the results by Liu et al.[44] match closely our DFT calculations at the PBE level with SOC included.[46] Additionally, in our simulation setup, we have used explicit 2D periodic boundary con-

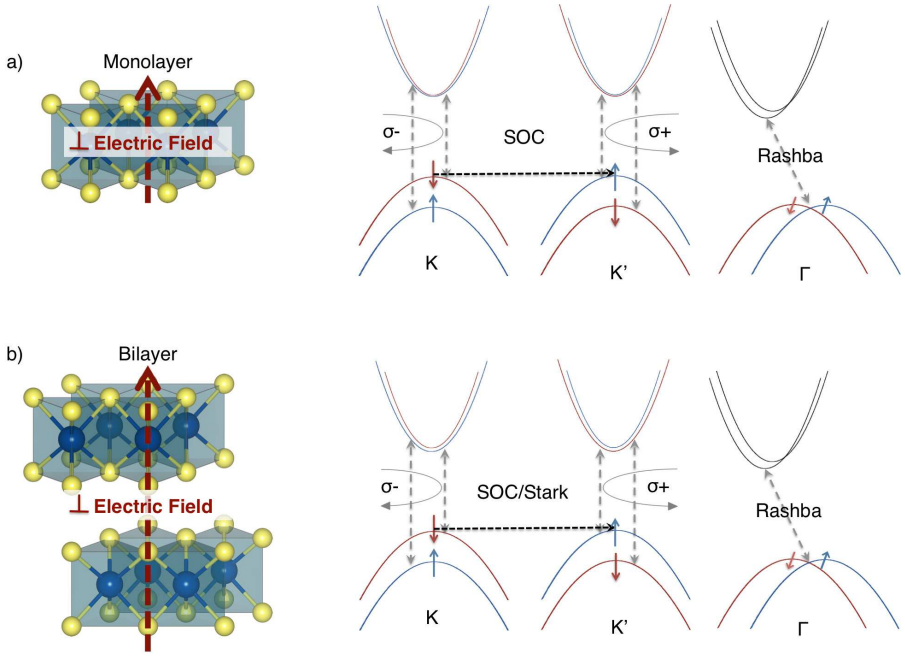

Fig. 5 Schematic representation of 2*H* TMC monolayer (ML; a) and bilayer (BL; b) together with the valence band maximum (VBM) and conduction band minimum (CBM) in the presence of an external electric field perpendicular to the basal planes. The electric field polarizes the planes and breaks the inversion and mirror symmetries. Spin-orbit coupling (SOC) at the *K* points occurs in the BLs, while it stays intact in the MLs. Additionally, at the Γ point, a Rashba spin-splitting occurs in the momentum space. The magnitude of the Rashba splitting depends on the electric field strength. Note, in the presence of perpendicular electric field, MLs and BLs are indirect gap semiconductors with VBM at the *K* and CBM halfway between *K* and Γ. Blue and red bands are spin-polarized.

ditions, thus avoiding spurious periodicity of the electric field normal to the planes. This approach is not, however, possible in the plane-wave based simulations, such as those of Ramasubramaniam et al.[18] While the band gap estimation with the applied electric field requires careful choice of the structural model and its periodicity, the spin-orbit band splittings are nevertheless well reproduced. In the VBM, Δ_{SO} reaches its maximum of 170 meV (420 meV) for molybdenum (tungsten) dichalcogenide BLs and stays unchanged for the whole range of applied field strengths.[46] This is in close agreement with Δ_{SO} reported by Ramasubramaniam et al.[18] for MoS_2 BLs, who obtained Δ_{SO} = 140 meV at similar field strength. For the WSe_2, Yuan et al.[24] have estimated Δ_{SO} of more than 200 meV for the $\boldsymbol{E}_\perp$ of 0.2 V Å^{-1} using DFT/PBE with plane-wave approach, in close agreement with our results.

The electric field causes also another phenomenon in the electronic band structure of 2D TMC materials. At the high-symmetry Γ point, $\boldsymbol{E}_\perp$ induces the so-called Rashba spin splitting.[42] The Rashba effect leads to a shift of spin-polarized bands in the momentum space in opposite directions (see Figure 7). Here, the SOC-induced spin-splitting is described by the Rashba energy (E_R) and the Rashba coupling parameter (α_R), which are related by:

$$\alpha_R = \frac{2E_R}{k_R}, \tag{5}$$

where k_R is the shift of bands in the momentum space. Under applied electric field, the Rashba effect is more pronounced for heavier TMC materials and increases with the field strength.

4 Heterostructures

Similar to the external perpendicular electric field, the electronic structure of TMC materials can be manipulated if a potential gradient normal to the basal planes is introduced to the system.[41] This can be achieved e.g. by the formation of heterostructures. TMC heterostructures were recently suggested on the basis of theory by Terrones et al.,[25] Komsa et al.,[48] and Cheng et al.[26] A schematic representation of TMC heterostructures in ML and BL forms is shown in Figure 8 together with the resulting band structures. It is important to note that, for most of the heterosystems, both MLs and BLs are direct band gap semiconductors with Δ located at the *K* point, and the lack of inversion symmetry induces large SO spin splitting. Similar to the electric field, the potential gradient results in the Rashba effect at the Γ point.

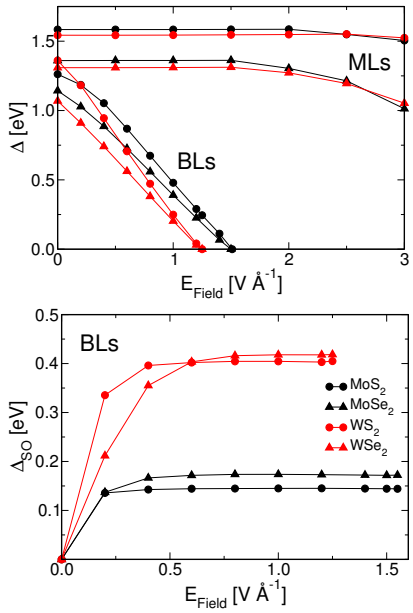

Fig. 6 Effect of an external electric field ($\boldsymbol{E}_{\perp}$) perpendicular to the basal planes of TMC MLs and BLs. The band gap (Δ) evolution as function of $\boldsymbol{E}_{\perp}$ (left), and the evolution of SO splitting (Δ_{SO}) BLs (right). Values taken from Refs. 45,46. Calculations at the DFT/PBE-D3(BJ) level with SR+SO.

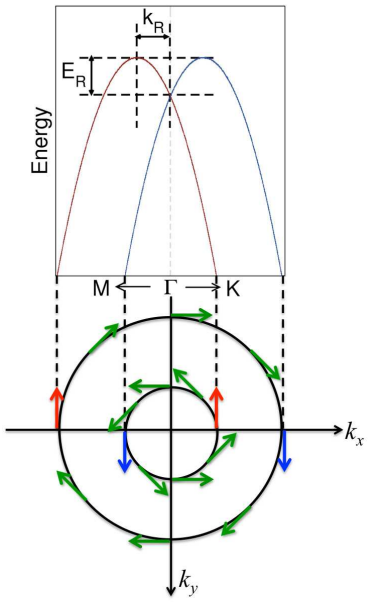

Fig. 7 Schematic representation of Rashba spin splitting in the momentum space at the Γ point. E_R and k_R denote the Rashba energy of the split states and the momentum, respectively. The spin orientation in the k_x-k_y plane of the momentum space is indicated for each split-band.

Cheng et al.[26] have calculated the electronic structures and the lattice dynamics of TXY (T transition metal atom, X and Y - chalcogen atoms) heterostructures (Figure 8 a) using a plane-wave approach and the DFT/PBE level of theory. The ML heterostructures are either direct or indirect band gap materials. From the phonon dispersion and the molecular dynamics simulations, Cheng et al.[26] showed that most of the systems are structurally stable, and the two unstable MoSSe and MoSeTe materials could be easily stabilized by external biaxial tensile strain. The SO spin splitting values of ML heterostructures at the *K* point in the valence and conduction bands are in between those corresponding to the pure MLs. For example, for MoSSe or WSeTe, the authors reported $\Delta_{\mathrm{SO}}^{VBM}$ ($\Delta_{\mathrm{SO}}^{CBM}$) of 170 (13) and 463 (43) meV, respectively, comparing with 150 (3), 188 (20), 473 (34), and 493 (51) meV for MoS_2, $MoSe_2$, WSe_2, and WTe_2, respectively (cf. Table 1).

Furthermore, Cheng et al.[26] have reported Rashba spin splitting at the Γ point in the valence band. The spin-resolved constant energy contours have almost perfect circular shapes for both inner and outer branches of the Rashba splitting (cf. Figure 7) in the $x-y$ plane, while in the out-of-plane direction, this effect is very low. The Rashba coupling parameters (α_R) are 2, 12, 4, 5, 14, and 10 meV Å, for MoSSe, MoSTe, MoSeTe, WSSe, WSTe, and WSeTe, respectively. These values are larger for heterostructures that consist of heavier elements, however, they are smaller than for typical narrow-gap semiconductors. The Rashba effect was found to be more sensitive to the difference in the distances of chalcogen atoms from the transition metal planes than to the atomic species. Although α_R is small, it is important to study the origin of the Rashba splitting, as it forms basis for the possible spin- and valleytronic applications.

We have recently studied the SO spin splitting in the valence and conduction bands of BL heterostructures, as suggested by Terrones et al.[25] and Komsa et al.[48] Here, the TMC BLs are formed from MLs of different stoichiometry (c.f. Figure 8 b). Considering the TMCs from group 6, many of the heterobilayers are direct band gap semiconductors. Our calculations (see Figure 9) suggest that Δ_{SO} values in the VBM at the *K* point are as large as the SOC observed for the heavier TMC MLs in the heterostructure. For example, for the MoS_2/WSe_2 and WS_2/WSe_2 BLs, the SO splittings reach 423 meV, similar to that of WSe_2 ML (428 meV). From the DFT/HSE calculations of MoS_2-WS_2 BL, Kosmider et al.[38] have obtained 578 meV SOC in comparison with the pure MLs of 202 and 577 meV, for MoS_2 and WS_2, respectively. Moreover, spin splittings, however much smaller, occur in the CBM.

In the heterobilayers, the Rashba effect is also present at the Γ point, however, it seems to be by one order of magnitude smaller than that in the ML heterostructures.

In our calculations of heterostructures, we have restricted ourselves to the smallest possible unit cells, which means that

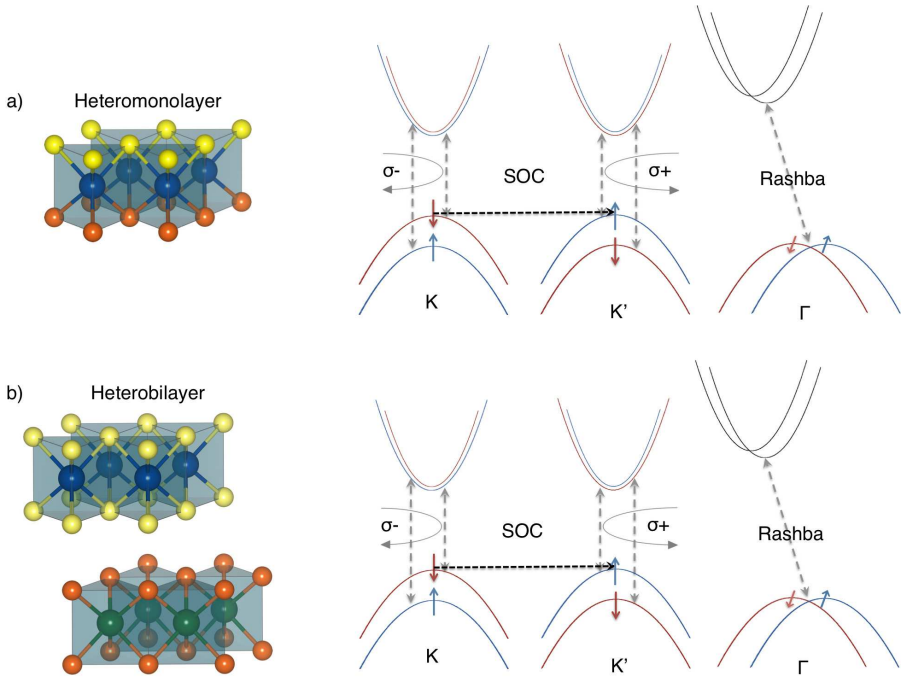

Fig. 8 Schematic representation of 2*H* TMC monolayer (ML; a) and bilayer (BL; b) together with the valence band maximum (VBM) and conduction band minimum (CBM) in the presence of a potential gradient perpendicular to the basal planes. Potential gradient occurs due to the heterostructures, either in a ML or BL. In both type of structures, the inversion and mirror symmetries are broken resulting in the spin-orbit coupling (SOC) at the *K* points. Additionally, at the Γ point, a Rashba spin-splitting occurs in the momentum space. Note, in the presence of potential gradient, both types of heterostructures are direct gap semiconductors with VBM and CBM at the *K* point. Blue and red bands are spin-polarized.

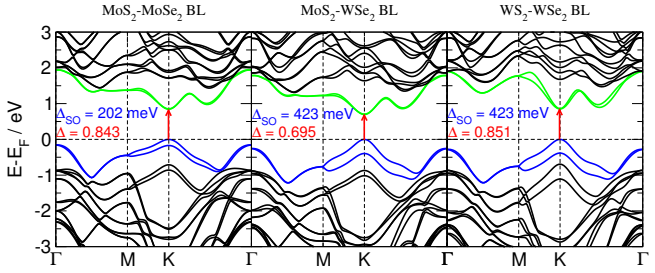

Fig. 9 Band structures of heterobilayers calculated with the SR+SO method and at the DFT/PBE-D3(BJ) level. Fundamental band gaps (Δ) and spin-orbit splittings (Δ_{SO}) are given for each system. Results taken from Refs. 37

the lattice vectors are optimized to average between those of the constituent MLs. This approach is commonly used to minimize the computational time and is known to give reasonable results in most cases. However, it also introduces a strain to the system and the electronic structure might be affected. Recently, Komsa et al.[48] have investigated the TMC heterobilayers using the plane-wave approach with the projector-augmented wave (PAW) scheme at the DFT/PBE level. They have used a supercell approach in such a way that the strain was minimized and smaller than 1%. Their MoS_2/WS_2 band structure showed that the system is an indirect band gap material with the *K* point strictly localized to one of the MLs: the VBM at the *K* point was completely localized to WS_2 and CBM to MoS_2. On the other hand, the $MoS_2/MoTe_2$ system is a direct band gap material, but again the VBM and CBM at the *K* point are localized to different MLs.

5 External Magnetic Field and Magnetoelectric Effects

Most recently, Kormányos et al.[40] have discussed the effect of a perpendicular magnetic field $\boldsymbol{B}_\perp$ on the intrinsic properties of TMC materials. They pointed out that $\boldsymbol{B}_\perp$ couples to the spin degree of freedom and breaks the valley degeneracy. The effective Hamiltonian of electrons in the conduction band was derived from the $\boldsymbol{k}\cdot\boldsymbol{p}$ model as follows:

$$\hat{H} = \hat{H}_{el} + \hat{H}_{vl} + \hat{H}_{sp} \tag{6}$$

$$\hat{H}_{el} = \frac{\hbar^2 \hat{q}_+ \hat{q}_-}{2m^*} + \frac{1+\tau}{2} sgn(\boldsymbol{B}_\perp)\hbar\omega_c \tag{7}$$

$$\hat{H}_{vl} = -\frac{1}{2}\tau\tilde{g}_{vl}\mu_B \boldsymbol{B}_\perp \tag{8}$$

$$\hat{H}_{sp} = \frac{1}{2}g_{SO}^{\perp}\mu_B \boldsymbol{s}_z \boldsymbol{B}_\perp \tag{9}$$

where $\hbar\omega_c = e\left|\boldsymbol{B}_\perp\right|/m^*$, $[\hat{q}_+, \hat{q}_-] = 2e\boldsymbol{B}_\perp/\hbar$, and $\tilde{g}_{vl}$ and $g_{SO}^{\perp}$ are the valley and out-of-plane effective spin g factors, respectively. The term $\sim \omega_c$ in the bulk introduces a shift in the index of the Landau levels, while $\hat{H}_{vl}$ breaks the symmetry of Landau levels. The $\hat{H}_{sp}$ term is similar to the Zeeman term:

$$\hat{H}_{sp} = \frac{1}{2}g_e\mu_B \boldsymbol{s}_z \boldsymbol{B}_\perp \tag{10}$$

with g_e being the free-electron g factor. This term describes the coupling between spin and magnetic field.

The effects of external perpendicular magnetic and electric fields on the electronic structure of TMC materials result in the splitting of the energy levels in different valleys and the Rashba spin-orbit coupling, respectively. The magnetic field couples to the spin degree of freedom, while the layer electrical polarization couples to the perpendicular electric field. This results in magnetoelectric effects, which were recently discussed by Gong et al.[23] for TMC BLs. Taking into account only the valence band, the authors have derived the hole Hamiltonian in the presence of both fields:

$$\hat{H}_v = -\lambda\,\tau_z\sigma_z\boldsymbol{s}_z + t_\perp\sigma_x + \boldsymbol{B}_x\boldsymbol{s}_x + \boldsymbol{B}_z\boldsymbol{s}_z + \boldsymbol{E}_z\sigma_z. \tag{11}$$

Note that $\boldsymbol{B}_z$ and $\boldsymbol{E}_z$ are equivalent to $\boldsymbol{B}_\perp$ and $\boldsymbol{E}_\perp$, respectively, while the in-plane magnetic field is taken along the x-axis. Gong et al. emphasize that the spin precession in a magnetic field can be controlled by a perpendicular electric field. In the presence of non-zero $\boldsymbol{E}_z$ and $\boldsymbol{B}_z$, the total effective field (its magnitude and direction) becomes valley dependent, with different oscillation frequencies in K and K'. This induces the so-called beating phenomenon in the precession of spin and electrical polarizations. Because of the beating effect, a finite spin polarization can arise from an initial state with zero net spin polarization.

6 Hall Effect

The absence of inversion symmetry in TMCs results not only in significant spin-orbit coupling, but it leads also to other interesting effects, such as spin, valley or charge Hall effects.[19,49,50] In the valley Hall effect (VHE), the carriers in different valleys flow to opposite sites in the presence of an in-plane electric field. This effect is accompanied by a spin Hall effect (SHE) when the systems are doped by electrons or holes. Due to the fact that the valley-dependent optical selection rule is spin-dependent, the carriers can be selectively excited by optical fields of different circular polarization (c.f. Figure 2) and frequencies.

The SHE and VHE are associated with the Berry curvature (Ω) and magnetic moment ($\mathbf{m}$). Time-reversal symmetry imposes that Ω and $\mathbf{m}$ have opposite signs in K and K' valleys. Following the derivation of Xiao et al.,[19] the Berry curvature can be defined as follows:

$$\Omega_n(\boldsymbol{k}) \equiv \hat{z}\cdot\nabla_{\boldsymbol{k}} \times \langle u_n(\boldsymbol{k})\left|i\nabla_k\right|u_n(\boldsymbol{k})\rangle \tag{12}$$

where $|u_n(\boldsymbol{k})\rangle$ is the periodic part of the Bloch function and n is the band index. Following Eq. 3, the Berry curvature for the conduction band can be written:

$$\Omega_c(\boldsymbol{k}) = -\tau\frac{2a^2t^2\Delta'}{\left[\Delta'^2 + 4a^2t^2k^2\right]^{2/3}}. \tag{13}$$

In the valence band holds $\Omega_v(\boldsymbol{k}) = -\Omega_c(\boldsymbol{k})$. In the K and K' valleys, the Berry curvature has opposite sign, while for the same valley, Ω is spin-dependent:

$$\Delta' \equiv \Delta - \tau\boldsymbol{s}_z\lambda. \tag{14}$$

Ω can be used to calculate the Hall conductivity:

$$\sigma_v^n = 2\int\frac{d\boldsymbol{k}}{(2\pi)^2}\left[f_{n,\uparrow}(\boldsymbol{k})\Omega_{n,\uparrow}(\boldsymbol{k}) + f_{n,\downarrow}(\boldsymbol{k})\Omega_{n,\downarrow}(\boldsymbol{k})\right] \tag{15}$$

and

$$\sigma_s^n = 2\int\frac{d\boldsymbol{k}}{(2\pi)^2}\left[f_{n,\uparrow}(\boldsymbol{k})\Omega_{n,\uparrow}(\boldsymbol{k}) - f_{n,\downarrow}(\boldsymbol{k})\Omega_{n,\downarrow}(\boldsymbol{k})\right] \tag{16}$$

where σ_v^n and σ_s^n are the valley and spin Hall conductivities in the units of $e/\hbar$ and $e/2$, respectively, and $f(\boldsymbol{k})$ is the Fermi-Dirac distribution function. Note that the integration is over the vicinity of the K or K' points.

If the system is doped with either holes or electrons, the Fermi energy (μ) shifts and the conductivities of holes ($\sigma_{s/v}^h$) and electrons ($\sigma_{s/v}^e$) can be calculated using

$$\sigma_s^h = \sigma_v^h = \frac{1}{\pi}\frac{\mu}{\Delta - \lambda}, \tag{17}$$

$$\sigma_s^e = \frac{1}{\pi}\frac{\lambda}{\Delta^2 - \lambda^2}\mu \;\text{ and }\; \sigma_v^e = \frac{1}{\pi}\frac{\Delta}{\Delta^2 - \lambda^2}\mu. \tag{18}$$

The carriers could be selectively excited (different combinations of spin and valley index) by optical fields with different optical circular polarization and frequency. Xiao et al.[19] pointed out that excitations with circular polarization generate the charge Hall current, while linear polarization will result in the spin and valley Hall currents. For the latter case, this means that spin-up electrons and holes in the K and K' valleys, respectively, will accumulate on one site, while their time-reversal counterparts will flow to the opposite site. This keeps both site charge neutral, but with net spin and valley polarizations.

From first principles, Feng et al.[50] have calculated the spin Hall effect and Berry curvatures of various TMC MLs. They have found that the intrinsic spin Hall conductivity is comparable to that of *p*- and *n*-doped III-V semiconductors. Moreover, the conductivities in the bulk systems are about an order of magnitude smaller than in monolayers.

Magnetoelectric effects were also studied in the MoS_2 BLs from polarization-resolved microphotoluminescence experiments and first principles simulations by Wu et al.[41] The authors show that the absorption circular dichroism and the orbital magnetic moment as function of the applied perpendicular electric field have distinct X-shape. This indicates that $\boldsymbol{E}_\perp$ breaks the BL inversion symmetry, modifies the dispersion of electron states, and controls the orbital magnetic moments of Bloch states. Wu et al.[41] concluded that the valley-contrasting magnetoelectric effect may be used as electrical control of the Berry curvature. Similar studies were performed by Cao et al.,[20] who showed that, when valley polarization is induced, only one of the valleys can have non-vanishing carrier populations, what leads to the Hall effect and magnetization without application of magnetic field. This was supported by the significant Berry curvature with opposite signs in the MoS_2 MLs.

7 Conclusions

Transition-metal chalcogenide systems have extraordinary intrinsic electronic properties that strongly depend on the number of layers and on the composition of the materials. These electronic properties can be easily controlled and tuned by external factors, in particular by electric and magnetic fields. TMC materials are widely investigated for potential applications in nano- and optoelectronics, especially for modern branches of flexible electronics, for spin- and valleytronics. The latter is possible because TMC monolayers offer giant spin-orbit spin splittings, which may reach about 500 meV at the valence band maximum for the tungsten-based systems. Due to the hexagonal symmetry, TMCs have two inequivalent energy valleys K and K' in the Brillouin zone. These valleys are coupled with the spin degree of freedom in the centro-asymmetric systems and, according to the optical selection rule, they will be populated with the spins of opposite signs.

When the TMC materials are exposed to an external electric field or any potential gradient is introduced to the system, the electronic structure changes significantly. While TMC monolayers are quite stable against commonly used gate voltages, the bilayers reduce their band gaps linearly with the field strength, eventually undergoing semiconductor-metal transition. Otherwise centro-symmetric bilayers become anisotropic in the presence of electric field, because their layers are polarized in different ways, what breaks the inversion symmetry and allows spin-orbit splitting to occur with values in the same range as for the corresponding monolayers. Therefore, TMC bilayers might be of interest as switching materials in the spin-based transistors. External fields or potential gradients give rise to phenomena such as Stark, Rashba or out-of-plane Zeeman effects. These effects can be observed by the changes in the band structures, especially at the high symmetry K and Γ points.

A static magnetic field controls the valley and spin magnetic moments in the real space, while perpendicular electric field controls the layer polarization. When a TMC system is exposed simultaneously to electric and magnetic fields, the spin and layers become valley dependent, giving rise to the spin polarization even for initial state with zero net polarization (beating phenomenon). Also magnetoelectric effects are observed for these systems: spin precession in a magnetic field can be controlled by an perpendicular electric field, and static a magnetic field can induce oscillations in layer polarization.

The results of electronic structure calculations of TMC materials are very sensitive to the computational approach, which therefore must be chosen carefully. Relativistic effects, especially the spin-orbit interaction, need to be taken into account to correctly describe the electronic structure. For example, to reproduce the direct band gap in the monolayers, scalar relativistic treatment of the core electrons is necessary. The choice of the simulation model is also critical, especially in the plane-wave calculations, where spurious interlayer interactions, due to the 3D periodicity, must be avoided. In heterostructures, extensive supercell models might be necessary to minimize in-plane strain resulting from the lattice mismatch. If the systems are exposed to the external fields, artifacts due to spurious periodicity in the direction of the field need to be avoided.

8 Acknlowledgements

Financial support by ONRG (N62909-13-1-N222), European Commission (MC-ITN MoWSeS, GA 317451) and Deutsche Forschungsgemeinschaft (DFG HE3543/18-1) is gratefully acknowledged.

References

1 A. K. Geim and K. S. Novoselov, *Nat. Mater.*, 2007, **6**, 183–191.
2 Q. H. Wang, K. Kalantar-Zadeh, A. Kis, J. N. Coleman and M. S. Strano, *Nat. Nanotechnol.*, 2012, **7**, 699–712.
3 V. Nicolosi, M. Chhowalla, M. G. Kanatzidis, M. S. Strano and J. N. Coleman, *Science*, 2013, **340**, 1226419–1–18.
4 M. Chhowalla, H. S. Shin, G. Eda, L.-J. Li, K. P. Loh and H. Zhang, *Nat. Chem.*, 2013, **5**, 263–75.
5 P. Miró, M. Audiffred and T. Heine, *Chem. Soc. Rev.*, 2014, In press.

6 X. Xu, W. Yao, D. Xiao and T. F. Heinz, *Nat. Phys.*, 2014, **10**, 343–350.

7 A. Splendiani, L. Sun, Y. B. Zhang, T. S. Li, J. Kim, C. Y. Chim, G. Galli and F. Wang, *Nano Lett.*, 2010, **10**, 1271–1275.

8 K. F. Mak, C. Lee, J. Hone, J. Shan and T. F. Heinz, *Phys. Rev. Lett.*, 2010, **105**, 136805–1–4.

9 A. Kuc, N. Zibouche and T. Heine, *Phys. Rev. B*, 2011, **83**, 245213–1–4.

10 B. Radisavljevic, A. Radenovic, J. Brivio, V. Giacometti and A. Kis, *Nat. Nanotechnol.*, 2011, **6**, 147–150.

11 G. Eda, T. Fujita, H. Yamaguchi, D. Voiry, M. Chen and M. Chhowalla, *ACS Nano*, 2012, **6**, 7311–7317.

12 R. Coehoorn, C. Haas, J. Dijkstra, C. J. F. Flipse, R. A. Degroot and A. Wold, *Phys. Rev. B*, 1987, **35**, 6195–6202.

13 J. N. Coleman, M. Lotya, A. ONeill, S. D. Bergin, P. J. King, U. Khan, K. Young, A. Gaucher, S. De, R. J. Smith, I. V. Shvets, S. K. Arora, G. Stanton, H.-Y. Kim, K. Lee, G. T. Kim, G. S. Duesberg, T. Hallam, J. J. Boland, J. J. Wang, J. F. Donegan, J. C. Grunlan, G. Moriarty, A. Shmeliov, R. J. Nicholls, J. M. Perkins, E. M. Grieveson, K. Theuwissen, D. W. McComb, P. D. Nellist and V. Nicolosi, *Science*, 2011, **331**, 568–571.

14 M. Ghorbani-Asl, N. Zibouche, M. Wahiduzzaman, A. F. Oliveira, A. Kuc and T. Heine, *Sci. Rep.*, 2013, **3**, 2961–1–2961–8.

15 J. Brivio, D. T. L. Alexander and A. Kis, *Nano Lett.*, 2011, **11**, 5148–5153.

16 P. Miró, M. Ghorbani-Asl and T. Heine, *Adv. Mater.*, 2013, **25**, 5473–5475.

17 Z. Y. Zhu, Y. C. Cheng and U. Schwingenschlögl, *Phys. Rev. B*, 2011, **84**, 153402–1–5.

18 A. Ramasubramaniam, D. Naveh and E. Towe, *Phys. Rev. B*, 2011, **84**, 205310–205325.

19 D. Xiao, G.-B. Liu, W. Feng, X. Xu and W. Yao, *Phys. Rev. Lett.*, 2012, **108**, 196802.

20 T. Cao, G. Wang, W. Han, H. Ye, C. Zhu, J. Shi, Q. Niu, P. H. Tan, E. Wang, B. Liu and J. Feng, *Nat. Commun.*, 2012, **3**, 1–5.

21 H. Zeng, J. Dai, W. Yao, D. Xiao and X. Cui, *Nature Nanotech.*, 2012, **7**, 490–493.

22 K. F. Mak, K. He, J. Shan and T. F. Heinz, *Nat. Nanotechnol.*, 2012, **7**, 494–498.

23 Z. Gong, G.-B. Liu, H. Yu, D. Xiao, X. Cui, X. Xu and W. Yao, *Nat. Commun.*, 2013, **4**, 2053.

24 H. Yuan, M. S. Bahramy, K. Morimoto, S. Wu, K. Nomura, B.-J. Yang, H. Shimotani, R. Suzuki, M. Toh, C. Kloc, X. Xu, R. Arita, N. Nagaosa and Y. Iwasa, *Nat. Phys.*, 2013, **9**, 563–569.

25 H. Terrones, F. López-Urías and M. Terrones, *Sci. Rep.*, 2013, **3**, 1549.

26 Y. C. Cheng, Z. Y. Zhu, M. Tahir and U. Schwingenschlögl, *Europhys. Lett.*, 2013, **102**, 57001.

27 L. Sun, J. Yan, D. Zhan, L. Liu, H. Hu, H. Li, B. K. Tay, J.-L. Kuo, C.-C. Huang, D. W. Hewak, P. S. Lee and Z. X. Shen, *Phys. Rev. Lett.*, 2013, **111**, 126801–126805.

28 J. A. Wilson and A. D. Yoffe, *Adv. Phys.*, 1969, **18**, 193–335.

29 P. Johari and V. B. Shenoy, *ACS Nano*, 2012, **6**, 5449–5456.

30 B. Liu, Y. Han, C. Gao, Y. Ma, G. Peng, B. Wu, C. Liu, Y. Wang, T. Hu, X. Cui, W. Ren, Y. Li, N. Su, H. L iu and G. Zou, *J. Phys. Chem. C*, 2010, **114**, 14251–14254.

31 P. Cudazzo, I. V. Tokatly and A. Rubio, *Phys. Rev. B*, 2011, **84**, 085406.

32 L. Wei, C. Jun-Fang, H. Qinyu and W. Teng, *Physica B: Condens. Matter*, 2010, **405**, 2498–2502.

33 H. S. S. R. Matte, A. Gomathi, A. K. Manna, D. J. Late, R. Datta, S. K. Pati and C. N. R. Rao, *Angew. Chem. Int. Ed.*, 2010, **49**, 4059–4062.

34 G. Arora, Y. Sharma, V. Sharma, G. Ahmed, S. K. Srivastava and B. L. Ahuja, *J. Alloys Compd.*, 2009, **470**, 452–460.

35 C. Ataca, H. Sahin and S. Ciraci, *J. Phys. Chem. C*, 2012, **116**, 8983–8999.

36 K. K. Kam and B. A. Parkinson, *J. Phys. Chem.*, 1982, **86**, 463–467.

37 N. Zibouche, A. Kuc, J. Musfeldt and T. Heine, *Annalen der Physik*, 2014, accepted.

38 K. Kośmider and J. Fernández-Rossier, *Physical Review B*, 2013, **87**, 75451.

39 K. Kośmider, J. W. González and J. Fernández-Rossier, *Phys. Rev. B*, 2013, **88**, 245436.

40 A. Kormányos, V. Zólyomi, N. D. Drummond and G. Burkard, *Phys. Rev. X*, 2014, **4**, 011034.

41 S. Wu, J. S. Ross, G.-B. Liu, G. Aivazian, A. M. Jones, Z. Fei, W. Zhu, D. Xiao, W. Yao, D. Cobden and X. Xu, *Nat. Phys.*, 2013, **9**, 149–153.

42 Y. A. Bychkov and E. I. Rashba, *JETP Lett.*, 1984, **39**, 78–81.

43 G. Dresselhaus, *Phys. Rev.*, 1955, **100**, 580–586.

44 Q. Liu, L. Li, Y. Li, Z. Gao, Z. Chen and J. Lu, *J. Phys. Chem. C*, 2012, **116**, 21556–21562.

45 N. Zibouche, P. Philipsen, T. Heine and A. Kuc, *Phys. Chem. Chem. Phys.*, 2014, **16**, 11251–11255.

46 N. Zibouche, P. H. T. Philipsen, A. Kuc and T. Heine, *Phys. Rev. B*, 2014, submitted.

47 J. Stark, *Ann. d. Phys.*, 1915, **48**, 193.

48 H.-P. Komsa and A. V. Krasheninnikov, *Phys. Rev. B*, 2013, **88**, 085318.

49 D. Xiao, W. Yao and Q. Niu, *Phys. Rev. Lett.*, 2007, **99**, 236809.
50 W. Feng, Y. Yao, W. Zhu, J. Zhou, W. Yao and D. Xiao, *Phys. Rev. B*, 2012, **86**, 165108.